Maxwell-Stefan-theory-based lattice Boltzmann model for diffusion in multicomponent mixtures

Zhenhua Chai,[1,2,*] Xiuya Guo,[1] Lei Wang,[3] and Baochang Shi[1,2,†]

[1]*School of Mathematics and Statistics, Huazhong University of Science and Technology, Wuhan 430074, China*

[2]*Hubei Key Laboratory of Engineering Modeling and Scientific Computing, Huazhong University of Science and Technology, Wuhan 430074, China*

[3]*School of Mathematics and Physics, China University of Geosciences, Wuhan, 430074, China*

(Received 8 October 2018; published 19 February 2019)

The phenomena of diffusion in multicomponent (more than two components) mixtures are universal in both science and engineering, and from the mathematical point of view, they are usually described by the Maxwell-Stefan (MS)-theory-based diffusion equations where the molar average velocity is assumed to be zero. In this paper, we propose a multiple-relaxation-time lattice Boltzmann (LB) model for the mass diffusion in multicomponent mixtures and also perform a Chapman-Enskog analysis to show that the MS continuum equations can be correctly recovered from the developed LB model. In addition, considering the fact that the MS-theory-based diffusion equations are just a diffusion type of partial differential equations, we can also adopt much simpler lattice structures to reduce the computational cost of present LB model. We then conduct some simulations to test this model and find that the results are in good agreement with the previous work. Besides, the reverse diffusion, osmotic diffusion, and diffusion barrier phenomena are also captured. Finally, compared to the kinetic-theory-based LB models for multicomponent gas diffusion, the present model does not include any complicated interpolations, and its collision process can still be implemented locally. Therefore, the advantages of single-component LB method can also be preserved in present LB model.

DOI: 10.1103/PhysRevE.99.023312

I. INTRODUCTION

Diffusion, an important transport process, has received increasing attention for its physical significance in the study of most chemical engineering and energy problems [1–4]. From the physical point of view, diffusion is the result of random molecular motion [1], while mathematically, diffusion can also be depicted by two classic continuum mechanical models [1–3,5], i.e., Fick's-law-based equations [6] and Maxwell-Stefan (MS)-theory-based diffusion equations [7,8]. In the first model, the diffusion flux of one component is assumed to be proportional to the negative of its concentration gradient, and the cross effects (or the influences of other components) in a system with more than two components are not included, although they are well-known to appear in reality. In the past decades, Fick's-law-based diffusion equations have been widely used to investigate the multicomponent diffusion problems for their simplicity, while they are only valid for the diffusion in binary mixtures or diffusion of a dilute species in a multicomponent system, and thus some curious phenomena caused by the cross effects in the multicomponent mixtures, including reverse diffusion (up-hill diffusion in direction of the concentration gradient), osmotic diffusion (diffusion without a concentration gradient), and diffusion barrier (no diffusion with a concentration gradient) [9,10], cannot be captured by this kind of diffusion equations [1–3]. To account for such complex diffusion phenomena observed in the multicomponent mixtures [2,10,11], MS-theory-based diffusion equations must be considered. However, MS-theory-based diffusion equations are nonlinear coupled partial differential equations, and usually it is difficult or even impossible to obtain their analytical solutions. For this reason, most available work focuses on the approximate solutions of such complicated partial differential equations. Basically, there are two possible ways that can be used to obtain the approximate solutions of the MS-theory-based diffusion equations. The first one is theoretical approach [1]. In this approach, usually the MS-theory-based diffusion equations are first linearized where the effective diffusivities are assumed to be constants, then some mathematical methods are applied to derive the solutions of the linearized equations [1,12,13]. Although this approach can be used to reveal the complex diffusion mechanisms in multicomponent mixtures [9–11,14], it is usually limited to one-dimensional problems and sometimes may also bring some undesirable errors due to the assumption of composite-independent effective diffusivities in the linearized equations [15]. The other one is numerical approach [16,17]. In the derivation of approximate solutions with this approach, there are no assumptions, but we need to develop some numerical schemes with certain truncation errors to discretize MS-theory-based diffusion equations. With the development of computer technology and scientific computing, this approach has become more popular in solving the MS-theory-based diffusion equations. Actually, some numerical methods, including the finite-difference method [18,19], finite-volume method [20–25], finite-element method [26–29], and

*hustczh@hust.edu.cn

†Corresponding author: shibc@hust.edu.cn

smoothed particle hydrodynamics method [30], have been developed to solve MS-theory-based diffusion equations.

As an alternative to the above-mentioned numerical methods for multicomponent diffusion problems, the lattice Boltzmann (LB) method [31,32], a mesoscopic numerical method developed from lattice gas automata [33] or continuum Boltzmann equation [34], has also been adopted to study the diffusion in multicomponent mixtures for its kinetic background [35,36]. Generally, there are three main kinds of LB models, i.e., kinetic-theory-based LB models [37–46], pseudopotential-based LB models [47–49], and free-energy-based LB models [50,51], that have been used for multicomponent diffusion problems. The LB models of the first kind are developed from some particular kinetic equations for multicomponent gas mixtures [35] and can also be viewed as a natural extension of the LB models for single-component fluid flows. Due to the solid physical background, these LB models have also been applied to investigate the multicomponent gas transport in complex porous media at pore scale level [52–56]. However, the LB models of this kind also have some limitations. For instance, when these LB models are adopted to study the diffusion in multicomponent mixtures with different molecular weights, some complicated interpolations [38,45,46], modifications on the equilibrium distribution function of the truncated Maxwellian form [38,41–43], or finite-difference techniques [39,40,44] must be needed. In the LB models of the second kind, a so-called pseudopotential is introduced to depict the interaction between different species [47,48]. To obtain correct macroscopic governing equations for multicomponent problems with different molecular weights, however, some modifications on equilibrium distribution functions and more discrete velocities are usually needed, as reported in Ref. [49]. In the last kind of LB models [50,51], some free-energy functions are introduced to give the chemical potentials and mean field forcing terms, and the equilibrium distribution functions and/or the forcing terms must be devised properly to recover the correct macroscopic equations.

Different from the models mentioned above, Hosseini *et al.* [57] also developed a LB model for multicomponent diffusion, which can be considered as a direct numerical solver to macroscopic governing equations for multicomponent fluid problems. To obtain correct governing equations from their LB model, a more complicated equilibrium distribution function including a gradient term is adopted, and to further determine the gradient term in the equilibrium distribution function, the local schemes developed in the framework of LB method [58–60] are used. We point out that, however, to obtain the gradient term related to species i in a multicomponent system, a linear system of equations rather than Eq. (28) in Ref. [57] must be solved. In this work, we would propose a MS-theory-based multiple-relaxation-time LB model for diffusion in multicomponent mixtures where a much simpler equilibrium distribution function is adopted. In our model, the coupling effects among different species are reflected through corresponding cross-collision terms, which is similar to that in the kinetic models for multicomponent gas mixtures [61]. In addition, through the Chapman-Enskog analysis, one can also show that the MS-theory-based diffusion equations can be recovered correctly from this model.

The rest of the paper is organized as follows. In Sec. II, the MS-theory-based equations for the diffusion in multicomponent mixtures are first introduced, then the LB model for these equations is developed in Sec. III. In Sec. IV, we present some numerical results and discussion, and finally, some conclusions are given in Sec. V.

II. MAXWELL-STEFAN THEORY OF THE DIFFUSION IN MULTICOMPONENT MIXTURES

For an ideal gas mixture composed of n chemical species, the molar concentration c_i of species i satisfies the following conservation equation [1,19,62]:

$$\partial_t c_i + \nabla \cdot \mathbf{N}_i = 0, \tag{1}$$

or

$$\partial_t c_i + \nabla \cdot (c_i \mathbf{u}) = -\nabla \cdot \mathbf{J}_i, \quad 1 \leqslant i \leqslant n, \tag{2}$$

where $\mathbf{N}_i = c_i \mathbf{u}_i$ is the molar flux of species i, $\mathbf{J}_i = c_i(\mathbf{u}_i - \mathbf{u})$ is the molar diffusion flux. $\mathbf{u}_i$ is the molar velocity, and $\mathbf{u}$ is the molar average velocity defined by

$$\mathbf{u} = \frac{1}{c_t} \sum_{i=1}^{n} c_i \mathbf{u}_i = \sum_{i=1}^{n} \xi_i \mathbf{u}_i, \quad c_t = \sum_{i=1}^{n} c_i, \tag{3}$$

where $\xi_i = c_i/c_t$ is the mole fraction of species i, and c_t is total molar concentration, a constant at the isobaric condition. Based on the definitions of molar diffusion flux and mole fraction, one can obtain the following relations:

$$\sum_{i=1}^{n} \mathbf{J}_i = 0, \tag{4a}$$

$$\sum_{i=1}^{n} \xi_i = 1. \tag{4b}$$

In the present work, we only consider the diffusion in multicomponent mixtures, and the molar average velocity $\mathbf{u}$ is assumed to be zero. In this case, Eqs. (1) and (2) can be rewritten as

$$\partial_t c_i = -\nabla \cdot \mathbf{J}_i, \quad 1 \leqslant i \leqslant n. \tag{5}$$

In the following, we would present some details on how to determine the molar diffusion flux $\mathbf{J}_i$ in the framework of MS theory.

In the MS theory, the thermodynamical driving force $\mathbf{d}_i$ exerted on species i is balanced by the total friction force of species i and other species. For an ideal gas mixture at the constant pressure P and temperature T, the driving force $\mathbf{d}_i$ takes the following form [1,2,62]:

$$\mathbf{d}_i = \frac{\xi_i}{RT} \nabla \mu_i = \nabla \xi_i, \tag{6}$$

where μ_i is the chemical potential, R is the gas constant. However, if the mutual friction force between species i and j is assumed to be proportional to the relative velocity and mole fraction [2,62], and based on the balance between the

driving forces, one can obtain

$$\nabla\xi_i = -\sum_{j\neq i}^{n}\sigma_{ij}\xi_i\xi_j(\mathbf{u}_i-\mathbf{u}_j) = -\sum_{j\neq i}^{n}\frac{\sigma_{ij}(\xi_j c_i\mathbf{u}_i-\xi_i c_j\mathbf{u}_j)}{c_t}, \tag{7}$$

where $\sigma_{ij}>0$ is the drag coefficient. Through incorporating the molar diffusion flux $\mathbf{J}_i$, we can also rewrite Eq. (7) as

$$\nabla\xi_i = -\sum_{j\neq i}^{n}\frac{\xi_j\mathbf{J}_i-\xi_i\mathbf{J}_j}{c_t D_{ij}}, \tag{8}$$

which is the so-called MS equation for species i. $D_{ij}=1/\sigma_{ij}$ is the MS diffusivity, and is also symmetric based on the fact $\sigma_{ij}=\sigma_{ji}$ [1,62].

Next, we would determine the explicit expression of molar diffusion flux $\mathbf{J}_i$ from the MS equations. Through a summation of Eq. (8) over i and with the help of Eq. (4b) or the symmetry of D_{ij}, we can first derive the following equation,

$$\sum_{i=1}^{n}\nabla\xi_i = -\sum_{i=1}^{n}\sum_{j\neq i}^{n}\frac{\xi_j\mathbf{J}_i-\xi_i\mathbf{J}_j}{c_t D_{ij}} = \mathbf{0}, \tag{9}$$

which indicates that the MS equations for all n species are linearly dependent. To eliminate the linear dependence, we can use Eqs. (4a) to remove the molar diffusion flux $\mathbf{J}_n$ and the equation related to $\nabla\xi_n$ from the MS Eqs. (8),

$$\begin{aligned}\nabla\xi_i &= -\frac{1}{c_t}\left(\mathbf{J}_i\sum_{j\neq i}^{n}\frac{\xi_j}{D_{ij}}-\xi_i\sum_{j\neq i}^{n}\frac{\mathbf{J}_j}{D_{ij}}\right)\\ &= -\frac{1}{c_t}\left(\mathbf{J}_i\sum_{j\neq i}^{n}\frac{\xi_j}{D_{ij}}-\xi_i\sum_{j\neq i}^{n-1}\frac{\mathbf{J}_j}{D_{ij}}+\frac{\xi_i}{D_{in}}\sum_{j=1}^{n-1}\mathbf{J}_j\right)\\ &= -\frac{1}{c_t}\left[\left(\frac{\xi_i}{D_{in}}+\sum_{j\neq i}^{n}\frac{\xi_j}{D_{ij}}\right)\mathbf{J}_i+\xi_i\sum_{j\neq i}^{n-1}\left(\frac{1}{D_{in}}-\frac{1}{D_{ij}}\right)\mathbf{J}_j\right],\\ &\quad 1\leqslant i\leqslant n-1,\end{aligned} \tag{10}$$

which can also be rewritten in a matrix form,

$$c_t\begin{pmatrix}\nabla\xi_1\\ \nabla\xi_2\\ \vdots\\ \nabla\xi_{n-1}\end{pmatrix} = -\mathbf{B}\begin{pmatrix}\mathbf{J}_1\\ \mathbf{J}_2\\ \vdots\\ \mathbf{J}_{n-1}\end{pmatrix}, \tag{11}$$

where $\mathbf{B}$ is a $(n-1)\times(n-1)$ matrix, and the element B_{ij} is given by

$$B_{ij} = \begin{cases}\xi_i\left(\frac{1}{D_{in}}-\frac{1}{D_{ij}}\right), & i\neq j,\\ \frac{\xi_i}{D_{in}}+\sum_{k\neq i}^{n}\frac{\xi_k}{D_{ik}}, & i=j.\end{cases} \tag{12}$$

If the matrix $\mathbf{B}$ is assumed to be invertible, then Eq. (11) can be written as

$$\begin{pmatrix}\mathbf{J}_1\\ \mathbf{J}_2\\ \vdots\\ \mathbf{J}_{n-1}\end{pmatrix} = -c_t\tilde{\mathbf{D}}\begin{pmatrix}\nabla\xi_1\\ \nabla\xi_2\\ \vdots\\ \nabla\xi_{n-1}\end{pmatrix}, \tag{13}$$

where $\tilde{\mathbf{D}}=\mathbf{B}^{-1}$ is the matrix of the effective diffusivity or generalized Fick diffusivity and is also a function of D_{ij} and ξ_i. From Eq. (13), we can express the molar diffusion flux $\mathbf{J}_i$ as

$$\mathbf{J}_i = -c_t\sum_{j=1}^{n-1}\tilde{D}_{ij}\nabla\xi_j, \quad 1\leqslant i\leqslant n-1, \tag{14}$$

which can be considered as the generalized Fick's law.

Substituting Eq. (14) into Eq. (5) and based on the definition of mole fraction, one can obtain the MS-theory-based diffusion equation for species i,

$$\partial_t\xi_i = \nabla\cdot\left(\sum_{j=1}^{n-1}\tilde{D}_{ij}\nabla\xi_j\right), \quad 1\leqslant i\leqslant n-1, \tag{15}$$

while for the species n, the mole fraction ξ_n can be determined directly by Eq. (4b). In the following, we adopt the MS-based diffusion Eq. (15) to study the diffusion in multicomponent mixtures. It should be noted that, however, in the derivation of the MS-theory-based diffusion Eq. (15), the assumptions of $\mathbf{u}=0$, constant temperature and pressure has been adopted, which gives rise to the zero total molar flux ($\mathbf{N}_t=\sum_{i=1}^{n}\mathbf{N}_i=c_t\mathbf{u}=0$) and constant total molar concentration ($c_t=$ constant). That is to say that the MS-theory-based diffusion equations are only suitable for the special multicomponent diffusion problems with zero total molar flux and constant total molar concentration.

Here we would also like to present some remarks on some special cases of the MS-theory-based Eq. (15), especially the matrix $\tilde{\mathbf{D}}$ and molar diffusion flux $\mathbf{J}_i$ [Eq. (14)].

Remark I. For a binary mixture, we can obtain the following relations:

$$\mathbf{J}_1 = -\mathbf{J}_2, \quad \xi_1+\xi_2=1, \quad D_{12}=D_{21}=\mathcal{D}, \tag{16}$$

where $\mathcal{D}$ is denoted as the diffusivity. Based on Eq. (16), one can rewrite the molar diffusion flux $\mathbf{J}_i$, i.e., Eq. (14), as

$$\mathbf{J}_i = -c_t\mathcal{D}\nabla\xi_i, \quad i=1,\ 2, \tag{17}$$

which is just the classic Fick's law.

Remark II. For a multicomponent system where all MS diffusivities D_{ij} $(1\leqslant i,j\leqslant n-1)$ are equal to each other, and are represented by $\mathcal{D}$, the matrix $\mathbf{B}$ [see Eq. (12)] and its inverse $\tilde{\mathbf{D}}$ can be simplified by

$$\mathbf{B} = \frac{1}{\mathcal{D}}\mathbf{I}, \quad \tilde{\mathbf{D}} = \mathcal{D}\mathbf{I}, \tag{18}$$

where $\mathbf{I}$ is the $(n-1)\times(n-1)$ unit matrix. With the help of Eq. (18), the molar diffusion flux $\mathbf{J}_i$ [see Eq. (14)] can be written in a much simpler form,

$$\mathbf{J}_i = -c_t\mathcal{D}\nabla\xi_i, \quad 1\leqslant i\leqslant n-1, \tag{19}$$

which is also consistent with the Fick's law.

Remark III. For a multicomponent system where the species i is dilute ($\xi_i\to 0$), the elements of matrix $\mathbf{B}$ (B_{ij}) can be approximated by

$$B_{ij} = \begin{cases}0, & i\neq j,\\ \mathcal{D}_{\text{eff}}, & i=j,\end{cases} \quad \mathcal{D}_{\text{eff}} = 1\Big/\sum_{k\neq i}^{n}\frac{\xi_k}{D_{ik}}, \tag{20}$$

where $\mathcal{D}_{\text{eff}}$ is the effective diffusivity. Then we can obtain the molar diffusion flux of specified dilute species i from Eq. (10),

$$\mathbf{J}_i = -c_t \mathcal{D}_{\text{eff}} \nabla \xi_i. \tag{21}$$

It is clear that Eq. (21) is similar to the Fick's law, but the effective diffusivity $\mathcal{D}_{\text{eff}}$ is a function of ξ_j $(j \neq i)$ and D_{ij} rather than a constant.

Remark IV. For a three-component system, the matrix $\mathbf{B}$ can be explicitly expressed as [62]

$$\mathbf{B} = \begin{bmatrix} \frac{1}{D_{13}} + \xi_2\left(\frac{1}{D_{12}} - \frac{1}{D_{13}}\right) & \xi_1\left(\frac{1}{D_{13}} - \frac{1}{D_{12}}\right) \\ \xi_2\left(\frac{1}{D_{23}} - \frac{1}{D_{12}}\right) & \frac{1}{D_{23}} + \xi_1\left(\frac{1}{D_{12}} - \frac{1}{D_{23}}\right) \end{bmatrix}, \tag{22}$$

where Eq. (4b) has been used. It is also easy to show that the matrix $\mathbf{B}$ is invertible since its determinant is not equal to zero, as seen below:

$$|\mathbf{B}| = \frac{\xi_1}{D_{12}D_{13}} + \frac{\xi_2}{D_{12}D_{23}} + \frac{\xi_3}{D_{13}D_{23}} > 0. \tag{23}$$

Then one can obtain the inverse of matrix $\mathbf{B}$,

$$\tilde{\mathbf{D}} = \frac{1}{\frac{\xi_1}{D_{12}D_{13}} + \frac{\xi_2}{D_{12}D_{23}} + \frac{\xi_3}{D_{13}D_{23}}} \begin{bmatrix} \frac{1}{D_{23}} + \xi_1\left(\frac{1}{D_{12}} - \frac{1}{D_{23}}\right) & \xi_1\left(\frac{1}{D_{12}} - \frac{1}{D_{13}}\right) \\ \xi_2\left(\frac{1}{D_{12}} - \frac{1}{D_{23}}\right) & \frac{1}{D_{13}} + \xi_2\left(\frac{1}{D_{12}} - \frac{1}{D_{13}}\right) \end{bmatrix}, \tag{24}$$

or equivalently,

$$\tilde{\mathbf{D}} = \frac{1}{\xi_1 D_{23} + \xi_2 D_{13} + \xi_3 D_{12}} \begin{bmatrix} D_{13}(\xi_1 D_{23} + (1-\xi_1)D_{12}) & \xi_1 D_{23}(D_{13} - D_{12}) \\ \xi_2 D_{13}(D_{23} - D_{12}) & D_{23}(\xi_2 D_{13} + (1-\xi_2)D_{12}) \end{bmatrix}, \tag{25}$$

which can be used to determine the explicit expression of molar diffusion flux $\mathbf{J}_i$.

III. LATTICE BOLTZMANN MODEL FOR MAXWELL-STEFAN-THEORY-BASED DIFFUSION EQUATIONS

The LB method, as one of kinetic-theory-based numerical approaches, has made great progress in the study of complex fluid flows in the past three decades [31,32,35,36,63–67], while simultaneously, it can also be considered as a general solver to nonlinear diffusion and convection-diffusion equations [59,68–78]. Based on the collision term, the basic LB models can be classified into three categories, i.e., the single-relaxation-time (SRT) LB model (or lattice BGK model) [79], the two-relaxation-time (TRT) LB model [80], and the multiple-relaxation-time (MRT) LB model (or generalized LB model) [81]. Here we consider the MRT-LB model for its advantages in generalization, stability, and accuracy [82–86].

Considering the fact that the MS-theory-based equations are only a special case of nonlinear coupled diffusion equations, some available LB models for diffusion or convection-diffusion equations can be extended to solve the MS-theory-based diffusion equations. In this work, we propose a MRT-LB model for these diffusion equations, and incorporate the cross collision terms in this model to reflect the coupling effects among different species which is similar to that in Ref. [70].

A. Multiple-relaxation-time lattice Boltzmann model

In the MRT-LB model for Eq. (15), the evolution equation can be written as [81,82]

$$\begin{aligned} &f_k^i(\mathbf{x} + \mathbf{c}_k \delta t,\ t + \delta t) \\ &= f_k^i(\mathbf{x},\ t) - \sum_{j=1}^{n-1} (\mathbf{M}^{-1} \mathbf{\Lambda}^{ij} \mathbf{M})_{k\alpha} \left[f_\alpha^j(\mathbf{x},\ t) - f_\alpha^{j,(\text{eq})}(\mathbf{x},\ t) \right], \\ &\quad 1 \leqslant i \leqslant n-1, \end{aligned} \tag{26}$$

where $f_k^i(\mathbf{x},\ t)$ $(k = 0,\ 1,\ \cdots,\ q-1$ or $1,\ 2\ \cdots,\ q$, with q representing the number of discrete velocity directions) is the distribution function of species i at position $\mathbf{x}$ and time t, $\mathbf{c}_k$ is the discrete velocity. $f_k^{i,(\text{eq})}(\mathbf{x},\ t)$ is the equilibrium distribution function, and for diffusion problems, it can be simply given by [69,76,78]

$$f_k^{i,(\text{eq})}(\mathbf{x},\ t) = \omega_k \xi_i, \tag{27}$$

where ω_k is the weight coefficient. In some commonly used DdQq (q velocity directions in d dimensional space) lattice models, the weight coefficient ω_k and discrete velocity $\mathbf{c}_k$ are defined as [78]

D1Q2:

$$\omega_1 = \omega_2 = \tfrac{1}{2}, \tag{28a}$$

$$\mathbf{c} = (1, -1)c, \tag{28b}$$

D1Q3:

$$\omega_0 = \tfrac{2}{3},\ \omega_1 = \omega_2 = \tfrac{1}{6}, \tag{29a}$$

$$\mathbf{c} = (0, 1, -1)c, \tag{29b}$$

D2Q4:

$$\omega_{i=1-4} = \frac{1}{4}, \tag{30a}$$

$$\mathbf{c} = \begin{pmatrix} 1 & 0 & -1 & 0 \\ 0 & 1 & 0 & -1 \end{pmatrix} c, \tag{30b}$$

D2Q5:

$$\omega_0 = \frac{1}{3},\ \omega_{i=1-4} = \frac{1}{6}, \tag{31a}$$

$$\mathbf{c} = \begin{pmatrix} 0 & 1 & 0 & -1 & 0 \\ 0 & 0 & 1 & 0 & -1 \end{pmatrix} c, \tag{31b}$$

D2Q9:

$$\omega_0 = \frac{4}{9},\ \omega_{i=1-4} = \frac{1}{9},\ \omega_{i=5-8} = \frac{1}{36}, \tag{32a}$$

$$\mathbf{c} = \begin{pmatrix} 0 & 1 & 0 & -1 & 0 & 1 & -1 & -1 & 1 \\ 0 & 0 & 1 & 0 & -1 & 1 & 1 & -1 & -1 \end{pmatrix} c, \tag{32b}$$

D3Q6:

$$\omega_{i=1-6} = \frac{1}{6}, \tag{33a}$$

$$\mathbf{c} = \begin{pmatrix} 1 & -1 & 0 & 0 & 0 & 0 \\ 0 & 0 & 1 & -1 & 0 & 0 \\ 0 & 0 & 0 & 0 & 1 & -1 \end{pmatrix} c, \tag{33b}$$

D3Q7:

$$\omega_0 = \frac{1}{4},\ \omega_{i=1-6} = \frac{1}{8}, \tag{34a}$$

$$\mathbf{c} = \begin{pmatrix} 0 & 1 & -1 & 0 & 0 & 0 & 0 \\ 0 & 0 & 0 & 1 & -1 & 0 & 0 \\ 0 & 0 & 0 & 0 & 0 & 1 & -1 \end{pmatrix} c, \tag{34b}$$

D3Q15:

$$\omega_0 = \frac{2}{9},\quad \omega_{i=1-6} = \frac{1}{9},\quad \omega_{i=7-14} = \frac{1}{72}, \tag{35a}$$

$$\mathbf{c} = \begin{pmatrix} 0 & 1 & -1 & 0 & 0 & 0 & 0 & 1 & 1 & 1 & 1 & -1 & -1 & -1 & -1 \\ 0 & 0 & 0 & 1 & -1 & 0 & 0 & 1 & -1 & -1 & 1 & 1 & -1 & -1 & 1 \\ 0 & 0 & 0 & 0 & 0 & 1 & -1 & 1 & -1 & 1 & -1 & 1 & -1 & 1 & -1 \end{pmatrix} c. \tag{35b}$$

$c = \delta x/\delta t$ is the lattice speed, and δx and δt are the lattice spacing and time step, respectively. We note that although there are some other lattice models [35,36], for the sake of brevity, they are not presented here. $\mathbf{M}$ is a $q \times q$ transformation matrix, and can be used to determine the moments of the distribution function f_k^i and equilibrium distribution function $f_k^{i,(\mathrm{eq})}$ in moment space,

$$\mathbf{m}^i := \mathbf{M}\mathbf{f}^{\mathbf{i}}, \quad \mathbf{m}^{i,(\mathrm{eq})} := \mathbf{M}\mathbf{f}^{i,(\mathrm{eq})}, \tag{36}$$

where $\mathbf{f}^i = (f_0^i,\ f_1^i,\ \cdots,\ f_{q-1}^i)^\top$ or $(f_1^i,\ f_2^i,\ \cdots,\ f_q^i)^\top$, $\mathbf{f}^{i,(\mathrm{eq})} = (f_0^{i,(\mathrm{eq})},\ f_1^{i,(\mathrm{eq})},\ \cdots, f_{q-1}^{i,(\mathrm{eq})})^\top$ or $(f_1^{i,(\mathrm{eq})},\ f_2^{i,(\mathrm{eq})},\ \cdots, f_q^{i,(\mathrm{eq})})^\top$ with $\top$ representing the transpose of a matrix. $\mathbf{\Lambda}^{ij} = \mathrm{diag}(\lambda_0^{ij},\ \lambda_1^{ij},\ \cdots,\ \lambda_{q-1}^{ij})$ or $\mathrm{diag}(\lambda_1^{ij},\ \lambda_2^{ij},\ \cdots,\ \lambda_q^{ij})$ is a diagonal relaxation matrix, and λ_k^{ij} is the relaxation parameter corresponding to the kth moment of distribution function.

For a specified one-, two-, or three-dimensional problem, one can first determine the corresponding lattice model, the transformation matrix $\mathbf{M}$ and the relaxation matrix $\mathbf{\Lambda}^{ij}$ [78,84], then the evolution Eq. (26) can be implemented with the following two steps:

Collision: $\mathbf{m}^{i,+}(\mathbf{x},\ t)$

$$= \mathbf{m}^i(\mathbf{x},\ t) - \sum_{j=1}^{n-1} \mathbf{\Lambda}^{ij}[\mathbf{m}^j(\mathbf{x},\ t) - \mathbf{m}^{j,(\mathrm{eq})}(\mathbf{x},\ t)], \tag{37a}$$

Propagation: $f_k^i(\mathbf{x} + \mathbf{c}_k\delta t,\ t + \delta t)$

$$= f_k^{i,+}(\mathbf{x},\ t), \qquad f_k^{i,+}(\mathbf{x},\ t) = \mathbf{M}^{-1}\mathbf{m}^{i,+}(\mathbf{x},\ t), \tag{37b}$$

where $f_k^{i,+}(\mathbf{x},\ t)$ is the post-collision distribution function. We note that although the present model is suitable for one-, two-, and three-dimensional multicomponent diffusion problems, for the sake of simplicity, here we only consider the two-dimensional MRT-LB model with D2Q5 lattice structure in which the transformation matrix $\mathbf{M}$ and relaxation matrix $\mathbf{\Lambda}^{ij}$ are given by [74,78]

$$\mathbf{M} = \mathbf{C}_d\mathbf{M}_0,\ \mathbf{C}_d = \mathrm{diag}(1, c, c, c^2, c^2),$$

$$\mathbf{M}_0 = \begin{pmatrix} 1 & 1 & 1 & 1 & 1 \\ 0 & 1 & 0 & -1 & 0 \\ 0 & 0 & 1 & 0 & -1 \\ 0 & 1 & -1 & 1 & -1 \\ -4 & 1 & 1 & 1 & 1 \end{pmatrix}, \tag{38a}$$

$$\mathbf{\Lambda}^{ij} = \mathrm{diag}\big(\lambda_0^{ij},\ \lambda_1^{ij},\ \lambda_1^{ij},\ \lambda_2^{ij},\ \lambda_2^{ij}\big). \tag{38b}$$

Based on Eq. (38a), we have

$$\mathbf{M}_0^{-1}\mathbf{\Lambda}^{ij}\mathbf{M}_0 = \mathbf{M}^{-1}\mathbf{\Lambda}^{ij}\mathbf{M}, \tag{39}$$

which can also be used to rewrite the evolution Eq. (26) in another form,

$$f_k^i(\mathbf{x} + \mathbf{c}_k\delta t,\ t + \delta t) = f_k^i(\mathbf{x},\ t) - \sum_{j=1}^{n-1} \big(\mathbf{M}_0^{-1}\mathbf{\Lambda}^{ij}\mathbf{M}_0\big)_{k\alpha} \times \big[f_\alpha^j(\mathbf{x},\ t) - f_\alpha^{j,(\mathrm{eq})}(\mathbf{x},\ t)\big]. \tag{40}$$

We also point out that in Eq. (38b), the second and third diagonal elements of relaxation matrix $\mathbf{\Lambda}^{ij}$ are denoted by a same parameter λ_1^{ij} since both of them correspond to the first-order moment of distribution function, while the fourth and fifth relaxation parameters represented by λ_2^{ij} corresponds to the second-order moment of distribution function. Besides, one can also show that if all the relaxation parameters are equal to each other, the MRT-LB model would reduce to the SRT-LB model [79], while if the relaxation parameters corresponding to odd and even-order moments are given by two different values (e.g., $\lambda_0^{ij} = \lambda_2^{ij} = \lambda_e^{ij}$, $\lambda_1^{ij} = \lambda_o^{ij}$), the MRT-LB model would be the same as the TRT-LB model [71].

In present MRT-LB model, the mole fraction ξ_i can be computed through a summation of the distribution function [76],

$$\xi_i(\mathbf{x},\ t) = \sum_{k=0}^{4} f_k^i(\mathbf{x},\ t), \tag{41}$$

the relation between the effective diffusivity $\tilde{D}_{ij}$ and elements of relaxation matrices can be expressed by the following Eq. (60).

In addition, it should be noted that in the MRT-LB model, besides the relaxation parameter λ_1^{ij} corresponding to effective diffusivity $\tilde{D}_{ij}$, there are also two free relaxation parameters that need to be determined. In the following simulations, the relaxation parameter λ_0^{ij} corresponding to the conservation variable is set to be $\lambda_0^{ij} = 1$ since it almost has no influence on the accuracy and stability of MRT-LB model [76,84]. The relaxation parameter λ_2^{ij} corresponding to the second-order moment, however, is a key parameter [84], and to eliminate the discrete effect of half-way bounce-back boundary condition, the following relations are adopted,

$$\lambda_2^{ij} = \begin{cases} \lambda_1^{ij}, & i \neq j, \\ 8\left(\lambda_1^{ij} - 2\right)/\left(\lambda_1^{ij} - 8\right), & i = j. \end{cases} \tag{42}$$

Finally, we point out that compared to the kinetic-theory-based LB models, the most striking feature of the present LB model is that it can readily handle the multicomponent diffusion problems with different molecular weights, and does not include any complicated interpolations.

B. The Chapman-Enskog analysis

We now conduct a detailed Chapman-Enskog analysis and show how to derive the MS-theory-based diffusion equations from present MRT-LB model. In the Chapman-Enskog analysis, the distribution function $f_k^i(\mathbf{x},\ t)$, the derivatives of time and space can be expanded as [31,32,35,36]

$$f_k^i = f_k^{i,(0)} + \varepsilon f_k^{i,(1)} + \varepsilon^2 f_k^{i,(2)} + \cdots, \tag{43a}$$

$$\partial_t = \varepsilon\partial_{t_1} + \varepsilon^2\partial_{t_2}, \qquad \nabla = \varepsilon\nabla_1 = \varepsilon\left(\partial_{x_1},\ \partial_{y_1}\right)^\top, \tag{43b}$$

where ε is a small parameter.

Taking the Taylor expansion to Eq. (26), we have

$$D_k f_k^i + \frac{\delta t}{2} D_k^2 f_k^i = -\sum_{j=1}^{n-1} (\mathbf{M}^{-1}\bar{\mathbf{\Lambda}}^{ij}\mathbf{M})_{k\alpha}\left[f_\alpha^j - f_\alpha^{j,(\mathrm{eq})}\right], \tag{44}$$

where $D_k = \partial_t + \mathbf{c}_k \cdot \nabla$, $\bar{\mathbf{\Lambda}}^{ij} = \mathbf{\Lambda}^{ij}/\delta t$. Substituting Eq. (43) into Eq. (44) yields the following equation:

$$\begin{aligned} &\varepsilon D_{k1} f_k^{i,(0)} + \varepsilon^2\left[\partial_{t_2} f_k^{i,(0)} + D_{i1} f_k^{i,(1)} + \frac{\delta t}{2} D_{k1}^2 f_k^{i,(0)}\right] \\ &= -\sum_{j=1}^{n-1} (\mathbf{M}^{-1}\bar{\mathbf{\Lambda}}^{ij}\mathbf{M})_{k\alpha}\left[f_\alpha^{j,(0)} + \varepsilon f_\alpha^{j,(1)} + \varepsilon^2 f_\alpha^{j,(2)} - f_\alpha^{j,(\mathrm{eq})}\right] \\ &\quad + O(\varepsilon^3), \end{aligned} \tag{45}$$

where $D_{k1} = \partial_{t_1} + \mathbf{c}_k \cdot \nabla_1$.

From Eq. (45), one can obtain the zeroth-, first-, and second-order equations in ε,

$$\varepsilon^0 : \sum_{j=1}^{n-1} (\mathbf{M}^{-1}\bar{\mathbf{\Lambda}}^{ij}\mathbf{M})_{k\alpha}\left[f_\alpha^{j,(0)} - f_\alpha^{j,(\mathrm{eq})}\right] = 0, \tag{46a}$$

$$\varepsilon^1 : D_{k1} f_k^{i,(0)} = -\sum_{j=1}^{n-1} (\mathbf{M}^{-1}\bar{\mathbf{\Lambda}}^{ij}\mathbf{M})_{k\alpha} f_\alpha^{j,(1)}, \tag{46b}$$

$$\begin{aligned} &\varepsilon^2 : \partial_{t_2} f_k^{i,(0)} + D_{k1} f_k^{i,(1)} + \frac{\delta t}{2} D_{k1}^2 f_k^{i,(0)} \\ &\quad = -\sum_{j=1}^{n-1} (\mathbf{M}^{-1}\bar{\mathbf{\Lambda}}^{ij}\mathbf{M})_{k\alpha} f_\alpha^{j,(2)}. \end{aligned} \tag{46c}$$

If we introduce the matrix $\tilde{\mathbf{\Lambda}}$,

$$\tilde{\mathbf{\Lambda}} = \begin{pmatrix} \mathbf{\Lambda}^{11} & \mathbf{\Lambda}^{12} & \cdots & \mathbf{\Lambda}^{1(n-1)} \\ \mathbf{\Lambda}^{21} & \mathbf{\Lambda}^{22} & \cdots & \mathbf{\Lambda}^{2(n-1)} \\ \vdots & \vdots & \vdots & \vdots \\ \mathbf{\Lambda}^{(n-1)1} & \mathbf{\Lambda}^{(n-1)2} & \cdots & \mathbf{\Lambda}^{(n-1)(n-1)} \end{pmatrix}, \tag{47}$$

and assume that the matrix is nonsingular, then one can obtain the following equation from Eq. (46a):

$$\varepsilon^0 : \quad f_k^{i,(0)} = f_k^{i,(\mathrm{eq})}. \tag{48}$$

Multiplying the transformation matrix $\mathbf{M}$ on both sides of the zeroth-, first-, and second-order equations in ε, i.e., Eqs. (48), (46b), and (46c), we have

$$\varepsilon^0 : \mathbf{m}^{i,(0)} = \mathbf{m}^{i,(\mathrm{eq})}, \tag{49a}$$

$$\varepsilon^1 : \mathbf{D}_1\mathbf{m}^{i,(0)} = -\sum_{j=1}^{n-1} \bar{\mathbf{\Lambda}}^{ij}\mathbf{m}^{j,(1)}, \tag{49b}$$

$$\begin{aligned} &\varepsilon^2 : \partial_{t_2}\mathbf{m}^{i,(0)} + \mathbf{D}_1\left(\mathbf{m}^{i,(1)} - \frac{1}{2}\sum_{j=1}^{n-1} \mathbf{\Lambda}^{ij}\mathbf{m}^{j,(1)}\right) \\ &\quad = -\sum_{j=1}^{n-1} \bar{\mathbf{\Lambda}}^{ij}\mathbf{m}^{j,(2)}, \end{aligned} \tag{49c}$$

where Eq. (49b) has been adopted to obtain Eq. (49c). $\mathbf{m}^{i,(k)} = \mathbf{M}\mathbf{f}^{i,(k)}$ $(k = 0,\ 1,\ 2)$ with $\mathbf{f}^{i,(k)} = (f_0^{i,(k)},\ \cdots,\ f_4^{i,(k)})^\top$. Based on Eqs. (27) and (49a), we can express $\mathbf{m}^{i,(k)}(k = 0,\ 1,\ 2)$ as

$$\begin{aligned} \mathbf{m}^{i,(0)} &= \xi_i\left(1,\ 0,\ 0,\ 0,\ -\tfrac{2}{3}c^2\right)^\top, \\ \mathbf{m}^{i,(1)} &= \left(0,\ m_1^{i,(1)},\ \ldots,\ m_4^{i,(1)}\right)^\top, \\ \mathbf{m}^{i,(2)} &= \left(0,\ m_1^{i,(2)},\cdots,\ m_4^{i,(2)}\right)^\top. \end{aligned} \tag{50}$$

$\mathbf{D}_1 = \partial_t\mathbf{I} + \mathbf{M}\mathrm{diag}(c_{0\alpha}\nabla_{0\alpha},\ \cdots,\ c_{4\alpha}\nabla_{4\alpha})\mathbf{M}^{-1}$, and $\mathbf{M}\mathrm{diag}(c_{0\alpha}\nabla_{0\alpha},\ \cdots,\ c_{4\alpha}\nabla_{4\alpha})\mathbf{M}^{-1}$ can also be determined

explicitly by

$$\mathbf{M}\mathrm{diag}(c_{0\alpha}\nabla_{0\alpha},\ \cdots,\ c_{4\alpha}\nabla_{4\alpha})\mathbf{M}^{-1} = \begin{pmatrix} 0 & \partial_x & \partial_y & 0 & 0 \\ \frac{2c^2}{5}\partial_x & 0 & 0 & \frac{1}{2}\partial_x & \frac{1}{10}\partial_x \\ \frac{2c^2}{5}\partial_y & 0 & 0 & -\frac{1}{2}\partial_y & \frac{1}{10}\partial_y \\ 0 & c^2\partial_x & -c^2\partial_y & 0 & 0 \\ 0 & c^2\partial_x & c^2\partial_y & 0 & 0 \end{pmatrix}. \quad (51)$$

Based on Eq. (49b), we can first derive the first-order equations in ε, but for simplicity, here only the first three that are used in the following analysis are presented:

$$\partial_{t_1}\xi_i = 0, \quad (52a)$$

$$\frac{c^2}{3}\partial_{x_1}\xi_i = -\frac{1}{\delta t}\sum_{j=1}^{n-1}\lambda_1^{ij}m_1^{j,(1)}, \quad (52b)$$

$$\frac{c^2}{3}\partial_{y_1}\xi_i = -\frac{1}{\delta t}\sum_{j=1}^{n-1}\lambda_1^{ij}m_2^{j,(1)}, \quad (52c)$$

where Eqs. (50) and (51) have been used. Similarly, from Eq. (49c), one can also derive the second-order equations in ε, but here we only present the first one corresponding to the conservative variable ξ_i,

$$\partial_{t_2}\xi_i + \partial_{x_1}\left(m_1^{i,(1)} - \frac{1}{2}\sum_{j=1}^{n-1}\lambda_1^{ij}m_1^{j,(1)}\right) + \partial_{y_1}\left(m_2^{i,(1)} - \frac{1}{2}\sum_{j=1}^{n-1}\lambda_1^{ij}m_2^{j,(1)}\right) = 0, \quad (53)$$

which can also be written in the matrix form,

$$\partial_{t_2}\xi + \partial_{x_1}\left(\mathbf{I} - \tfrac{1}{2}\mathbf{\Lambda}_1\right)\mathbf{m}_1^{(1)} + \partial_{y_1}\left(\mathbf{I} - \tfrac{1}{2}\mathbf{\Lambda}_1\right)\mathbf{m}_2^{(1)} = 0, \quad (54)$$

where ξ, $\mathbf{m}_k^{(1)}$ $(k = 1,\ 2)$ and $\mathbf{\Lambda}_1$ are defined by

$$\xi = (\xi_1,\ \cdots,\ \xi_{n-1})^\top, \quad (55a)$$

$$\mathbf{m}_k^{(1)} = \left(m_k^{1,(1)},\ \cdots,\ m_k^{n-1,(1)}\right)^\top, \quad (55b)$$

$$\mathbf{\Lambda}_1 = \begin{pmatrix} \lambda_1^{11} & \lambda_1^{12} & \cdots & \lambda_1^{1(n-1)} \\ \lambda_1^{21} & \lambda_1^{22} & \cdots & \lambda_1^{2(n-1)} \\ \vdots & \vdots & \vdots & \vdots \\ \lambda_1^{(n-1)1} & \lambda_1^{(n-1)2} & \cdots & \lambda_1^{(n-1)(n-1)} \end{pmatrix}. \quad (55c)$$

However, from Eqs. (52b) and (52c), one can also obtain $\mathbf{m}_1^{(1)}$ and $\mathbf{m}_2^{(1)}$,

$$\mathbf{m}_1^{(1)} = -\frac{c^2}{3}\delta t\,\mathbf{\Lambda}_1^{-1}\partial_{x_1}\xi, \quad (56)$$

$$\mathbf{m}_2^{(1)} = -\frac{c^2}{3}\delta t\,\mathbf{\Lambda}_1^{-1}\partial_{y_1}\xi, \quad (57)$$

where $\mathbf{\Lambda}_1$ has been assumed to be invertible. Substituting Eqs. (56) and (57) into Eq. (54) leads to the following result:

$$\partial_{t_2}\xi = \partial_{x_1}\left[\frac{c^2}{3}\delta t\left(\mathbf{\Lambda}_1^{-1} - \frac{1}{2}\mathbf{I}\right)\partial_{x_1}\xi\right] + \partial_{y_1}\left[\frac{c^2}{3}\delta t\left(\mathbf{\Lambda}_1^{-1} - \frac{1}{2}\mathbf{I}\right)\partial_{y_1}\xi\right] = 0, \quad (58)$$

from which one can also obtain the equation for species i,

$$\partial_{t_2}\xi_i = \nabla_1\cdot\left(\sum_{j=1}^{n-1}\tilde{D}_{ij}\nabla_1\xi_j\right), \quad (59)$$

where the diffusivity $\tilde{D}_{ij}$ or the matrix $\tilde{\mathbf{D}}$ are given by

$$\tilde{D}_{ij} = \frac{c^2}{3}\delta t\left(\mathbf{\Lambda}_1^{-1} - \frac{1}{2}\mathbf{I}\right)_{ij}, \quad \tilde{\mathbf{D}} = \frac{c^2}{3}\delta t\left(\mathbf{\Lambda}_1^{-1} - \frac{1}{2}\mathbf{I}\right). \quad (60)$$

Through a combination of Eqs. (52a) and (59), i.e., $\varepsilon\times(52a) + \varepsilon^2\times(59)$, we can correctly recover the MS-theory-based diffusion equation for species i [see Eq. (15)].

Now let us focus on how to calculate the gradient term $\nabla\xi_i$ $(1\leqslant i\leqslant n-1)$, which can be used to determine the diffusion flux [see Eq. (13)]. Generally speaking, there are two possible ways that can be applied to obtain $\nabla\xi_i$. The first one is to directly use the nonlocal finite-difference scheme to compute $\nabla\xi_i$, while the second is, in the framework of LB method, to calculate $\nabla\xi_i$ locally through the nonequilibrium part of the distribution function [59,60]. Actually, the second approach has also been adopted to improve stability of LB method [87] and to predict effective diffusivity of porous media [86].

Here we only consider the latter one for its locality in the computation of gradient term. If we multiply ε on both sides of Eqs. (52b) and (52c), then one can obtain

$$\frac{c^2}{3}\partial_x\xi_i = -\frac{1}{\delta t}\sum_{j=1}^{n-1}\lambda_1^{ij}\left[m_1^j - m_1^{j,(0)}\right] = -\frac{1}{\delta t}\sum_{j=1}^{n-1}\lambda_1^{ij}m_1^j = -\frac{1}{\delta t}\sum_{j=1}^{n-1}\lambda_1^{ij}\sum_{k=0}^{4}\mathbf{c}_{k,x}f_k^j, \quad (61a)$$

$$\frac{c^2}{3}\partial_y\xi_i = -\frac{1}{\delta t}\sum_{j=1}^{n-1}\lambda_1^{ij}\left[m_2^j - m_2^{j,(0)}\right] = -\frac{1}{\delta t}\sum_{j=1}^{n-1}\lambda_1^{ij}m_2^j = -\frac{1}{\delta t}\sum_{j=1}^{n-1}\lambda_1^{ij}\sum_{k=0}^{4}\mathbf{c}_{k,y}f_k^j, \quad (61b)$$

where the assumptions of $\varepsilon m_1^{j,(1)} = m_1^j - m_1^{j,(0)}$ and $\varepsilon m_2^{j,(1)} = m_2^j - m_2^{j,(\mathrm{eq})}$ [59,60,76], and the fact $m_1^{j,(0)} = m_2^{j,(0)} = 0$ have been adopted. From the above equations, we can finally determine $\nabla\xi_i = (\partial_x\xi_i,\ \partial_y\xi_i)^\top$,

$$\nabla\xi_i = -\frac{3}{\delta t c^2}\sum_{j=1}^{n-1}\lambda_1^{ij}\sum_{k=0}^{4}\mathbf{c}_k f_k^j, \quad (62)$$

which can be further used to calculate the diffusion flux $\mathbf{J}$ [see Eq. (13)].

IV. NUMERICAL VALIDATION AND DISCUSSION

In this section, several benchmark problems that appeared in Refs. [1,11,17,19,44,91] are used to validate present MRT-LB model. The codes are written in C, and all the computations are conducted on an Intel Core (TM) i7-6700 processor with four cores of 3.40 GHz and 16 GB RAM. In our simulations, the halfway anti-bounce-back scheme is used for the Dirichlet boundary condition [88–90],

$$f_k^i(\mathbf{x}_f,\ t+\delta t) = -f_{\bar{k}}^{i,+}(\mathbf{x}_f,\ t) + 2\omega_{\bar{k}}\xi_{i,b}, \tag{63}$$

while for no-flux boundary condition, the standard halfway bounce-back scheme is adopted [74,88],

$$f_k^i(\mathbf{x}_f,\ t+\delta t) = f_{\bar{k}}^{i,+}(\mathbf{x}_f,\ t), \tag{64}$$

where $f_k^i(\mathbf{x}_f,\ t+\delta t)$ is the unknown distribution function at the boundary node $\mathbf{x}_f$. $\xi_{i,b}$ is the mole fraction at the boundary, specified by the Dirichlet boundary condition, and $\bar{k}$ is the opposite direction of k. In the initialization process, the distribution function is given by its equilibrium part,

$$f_k^i(\mathbf{x},\ t)|_{t=0} = f_k^{i,(\mathrm{eq})}(\mathbf{x},\ t)|_{t=0} = \omega_k\xi_i|_{t=0}. \tag{65}$$

Additionally, to quantitatively measure the deviation between the numerical and analytical solutions, the relative error based on L^2 norm is used here,

$$E(\phi) = \sqrt{\frac{\sum_{(x,\ y)} |\phi_a(x,\ y,\ t) - \phi_n(x,\ y,\ t)|^2}{\sum_{(x,\ y)} |\phi_a(x,\ y,\ t)|^2}}, \tag{66}$$

where ϕ_a and ϕ_n denote the analytical and numerical results of the variable ϕ (e.g., the mole fraction ξ_i or one element of the diffusion flux $\mathbf{J}_i$).

A. A simple two-component diffusion problem

We first consider a simple two-component diffusion problem with a constant diffusivity $\mathcal{D}$ [see Eq. (16)] [91], which is also used to test the kinetic-theory-based LB models [44,45]. For this problem, the MS-theory-based diffusion equation would reduce to the Fick's-law-based conservation equation. For simplicity, here we only consider the mole fraction ξ_1 since the mole fraction ξ_2 can be obtained by $\xi_2 = 1 - \xi_1$. Under the following initial and boundary conditions,

$$t = 0:\ \xi_1 = C_0,\ x < 0,\ \xi_1 = C_1,\ x \geqslant 0, \tag{67a}$$

$$x = -\infty,\ \xi_1 = C_0,\quad x = +\infty,\ \xi_1 = C_1, \tag{67b}$$

one can obtain the analytical solutions of ξ_1 and diffusion flux $\mathbf{J}_1$,

$$\xi_1 = \frac{C_0 + C_1}{2} + \frac{C_1 - C_0}{2}\mathrm{erf}\left(\frac{x}{2\sqrt{\mathcal{D}t}}\right), \tag{68a}$$

$$\mathbf{J}_1 = -D\nabla\xi_1 = -\frac{C_1 - C_0}{2}\sqrt{\frac{\mathcal{D}}{\pi t}}e^{-\frac{x^2}{4\mathcal{D}t}}, \tag{68b}$$

where erf is the error function, and is defined by

$$\mathrm{erf}(y) = \frac{2}{\sqrt{\pi}}\int_0^y e^{-\eta^2}d\eta. \tag{69}$$

In the following, we consider the problem with the diffusivity $\mathcal{D} = 0.05$, $C_0 = 0.9$, $C_1 = 0.1$, and adopt the periodic boundary condition in y direction. The computational domain is fixed to be $[-6,\ 6] \times [-1,\ 1]$, and to ensure our simulations to be consistent with the physical problem, $x/2\sqrt{\mathcal{D}t}$ should be large enough. We first performed some simulations with the lattice size 240×40 and the relaxation parameter $\lambda_1^{11} = 1.25$, and presented the results at different time in Figs. 1 and 2. As seen from these two figures, the numerical results of mole fraction ξ_1 and diffusion flux $\mathbf{J}_1$ are in good agreement with the corresponding analytical solutions.

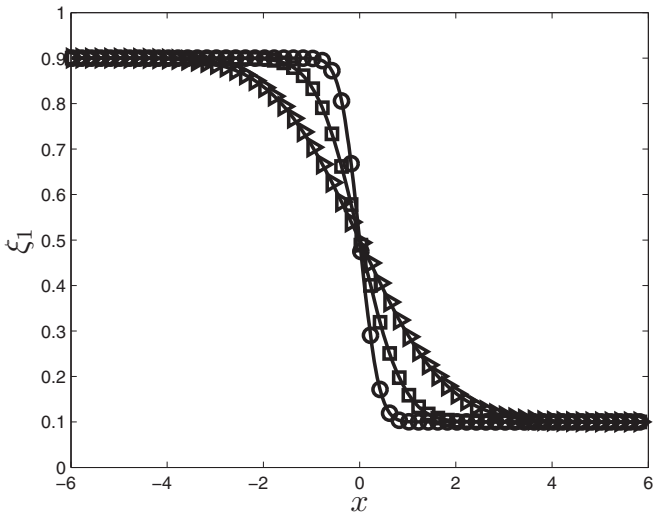

FIG. 1. The profiles of mole fraction ξ_1 at different time [Solid line: Eq. (68a), ◯: $t = 1.0$, □: $t = 5.0$, ▷: $t = 20.0$].

Then we also conducted several simulations with the SRT-LB model, in which $\lambda_0^{11} = \lambda_1^{11} = \lambda_2^{11} = 1.25$, and presented a comparison between these two LB models in Table I. From this table, one can find that the results of MRT-LB model is more accurate than the SRT-LB model, which is mainly caused by the adoption of Eq. (42) in the MRT-LB model. In addition, the computational costs of the SRT-LB and MRT-LB models are also measured at $t = 20$, and they are 5.639 and

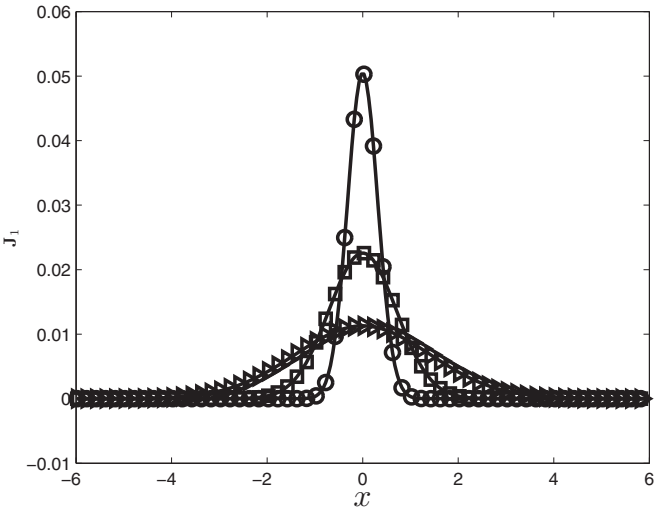

FIG. 2. The profiles of diffusion flux ξ_1 at different time [Solid line: Eq. (68b), ◯: $t = 1.0$, □: $t = 5.0$, ▷: $t = 20.0$].

TABLE I. A comparison between the errors of MRT-LB and SRT-LB models for mole fraction ξ_1 and flux $\mathbf{J}_1$.

	MRT-LB model		SRT-LB model	
Time	$E(\xi_1)$	$E(\mathbf{J}_1)$	$E(\xi_1)$	$E(\mathbf{J}_1)$
$t = 1$	1.4986×10^{-5}	2.7702×10^{-4}	1.1792×10^{-4}	1.0622×10^{-3}
$t = 5$	4.5260×10^{-6}	5.5143×10^{-5}	3.5758×10^{-5}	2.1227×10^{-4}
$t = 20$	2.8366×10^{-6}	4.6922×10^{-5}	1.3219×10^{-5}	6.7868×10^{-5}

6.920 s, respectively. These results show that the MRT-LB model is about 18.5% slower than the SRT-LB model in terms of CPU time, which is also consistent with the results reported in Ref. [83].

This problem is also adopted to test convergence rate of the MRT-LB model. To this end, we carried out some simulations under different lattice sizes ($\delta x = 1/10,\ 1/20,\ 1/30,\ 1/40$), and the errors of mole fraction ξ_1 and diffusion flux $\mathbf{J}_1$ are shown in Figs. 3 and 4 where the effects of relaxation parameter λ_1^{11} are also considered. As shown in these two figures, the MRT-LB model has a second-order convergence rate in space, both for mole fraction ξ_1 and diffusion flux $\mathbf{J}_1$. Besides, it is also found that although the relaxation parameter λ_1^{11} has some influences on the results of mole fraction ξ_1 and diffusion flux $\mathbf{J}_1$, it does not affect the second-order accuracy of MRT-LB model.

B. A three-component coupling diffusion problem

We continue to consider a three-component coupling diffusion problem [17,19] that is a close approximation to the classic experiment conducted by Duncan and Toor [10]. In the study of this problem, the diffusivities are set to be $D_{12} = D_{13} = 0.833$ and $D_{23} = 0.168$, the physical domain of the problem is $[0,\ 1] \times [0,\ 1]$, and the initial and boundary conditions of ξ_1 and ξ_2 are given by

$$\xi_1 = \begin{cases} 0.8, & 0 \leqslant x < 0.25, \\ 1.6(0.75 - x), & 0.25 \leqslant x < 0.75, \\ 0, & 0.75 \leqslant x \leqslant 1, \end{cases} \tag{70a}$$

$$\xi_2 = 0.2, \quad 0 \leqslant x \leqslant 1, \tag{70b}$$

$$x = 0, \quad \mathbf{J}_1 = \mathbf{J}_2 = 0, \quad x = 1, \quad \mathbf{J}_1 = \mathbf{J}_2 = 0, \tag{71a}$$

$$\xi_i|_{y=0} = \xi_i|_{y=1}\ (i = 1,\ 2,\ 3). \tag{71b}$$

Under the condition of $D_{12} = D_{13}$, one can rewrite Eq. (24) as

$$\tilde{\mathbf{D}} = \begin{pmatrix} D_{12} & 0 \\ \beta\xi_2\left(1 - \frac{D_{12}}{D_{23}}\right) & \beta \end{pmatrix}, \tag{72}$$

where the parameter β is defined by

$$\beta = \left[\frac{1}{D_{23}} + \xi_1\left(\frac{1}{D_{12}} - \frac{1}{D_{23}}\right)\right]^{-1}. \tag{73}$$

We carried out some simulations with the lattice size 200×200 and presented some results in Figs. 5–9. From the Figs. 5–7, one can first observe that the numerical results at $x = 0.72$ are very close to those reported in some previous work [17,19]. Then let us focus on the changes of mole fraction, diffusion flux, and the negative of mole fraction gradient in time. As shown in Fig. 5, the mole fraction ξ_1 normally increases in time and finally approaches to the equilibrium

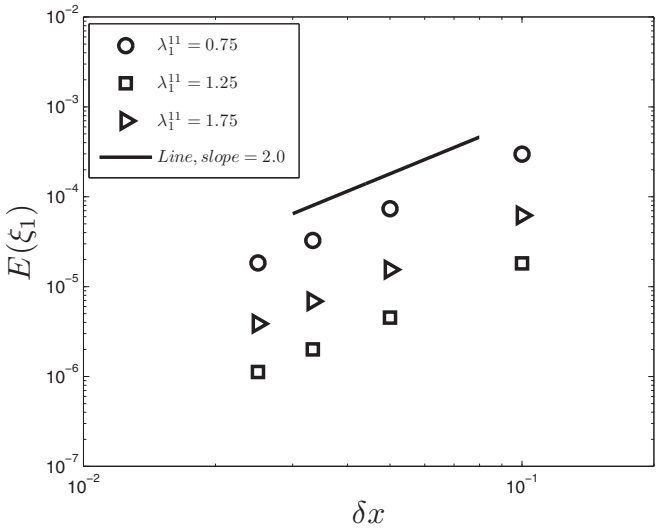

FIG. 3. The errors of MRT-LB model for mole fraction ξ_1 at the time $t = 5$, the slope of the inserted line is 2.0, which indicates that the MRT-LB model has a second-order convergence rate in space.

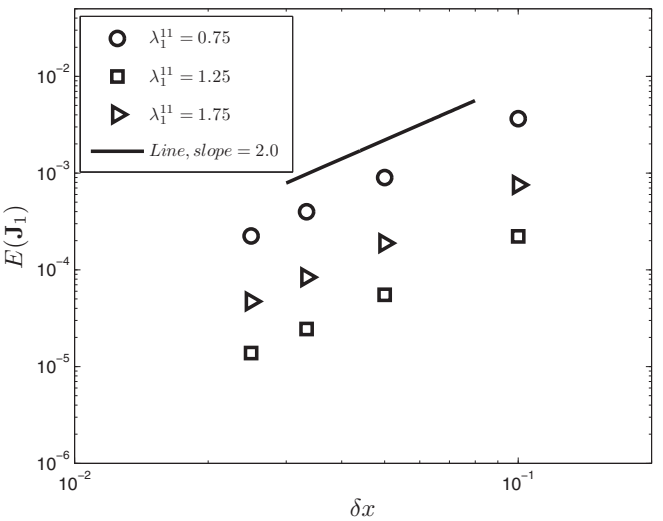

FIG. 4. The errors of MRT-LB model for mole fraction $\mathbf{J}_1$ at the time t = 5, the slope of the inserted line is 2.0, which indicates that the MRT-LB model has a second-order convergence rate in space.

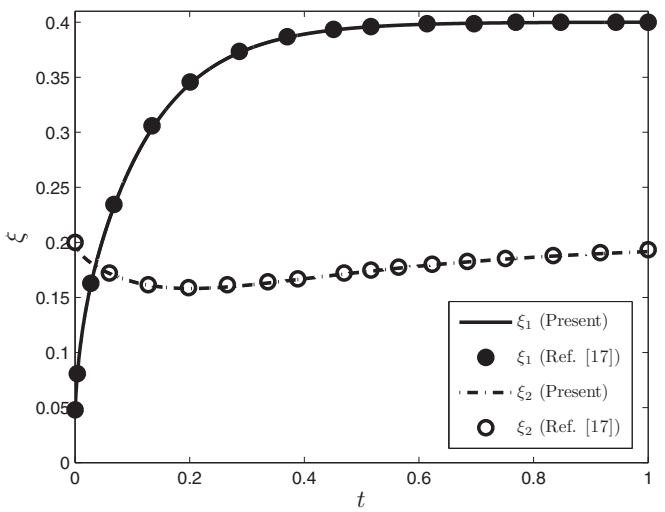

FIG. 5. The mole fraction ξ_i $(i = 1,\ 2)$ at different time $(x = 0.72)$.

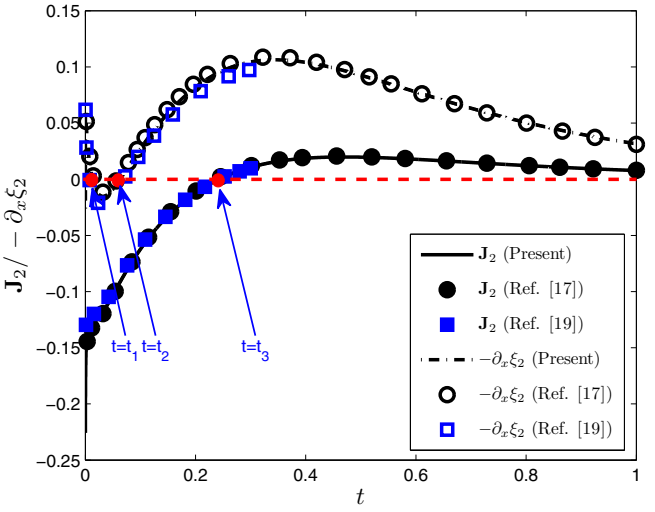

FIG. 7. The diffusion flux $\mathbf{J}_2$ and the negative of mole fraction gradient $(-\partial_x\xi_2)$ at different time $(x = 0.72)$.

value $\xi_1^* = 0.4$ [also see Fig. 8(a) where the time t is increased to $t = 5$]. Besides, from Fig. 6, we can also observe that the diffusion flux $\mathbf{J}_1$ and the negative of mole fraction gradient $(-\partial_x\xi_1)$ decrease with the increase of time and becomes zero when t is large enough [see Figs. 8(b) and 8(c)]. These results on species 1 are consistent with the theory based on Fick's law since there are no cross effects induced by other species $(D_{12} = D_{13})$. However, from Fig. 5, one can also find some curious results on the mole fraction ξ_2 which are caused by the cross effects from other species, and can also be seen clearly from Eq. (14) under the specified matrix $\mathbf{D}$ given by Eq. (72). Initially, the mole fraction ξ_2 is at its equilibrium value $\xi_2^* = 0.2$, based on the Fick's law, there should be no mass diffusion for species 2. The mole fraction ξ_2 first decreases, however, reaching the minimum value $\xi_2^{\min} = 0.1581$ at about $t = 0.2$. After that, the mole fraction ξ_2 begins to increase, reaching the equilibrium value $\xi_2^* = 0.2$ when the time is large enough [see Fig. 9(a)]. We note that these interesting results are similar to the classic experimental results reported in Ref. [10] and cannot be depicted by the theory based on the simple Fick's law. To elucidate these phenomena more clearly, we also plotted the variations of diffusion flux and negative of the mole fraction gradient in time in Fig. 7, from which one can find that when the time is located in the range of $0 < t < t_1$ or $t_2 < t < t_3$, the so-called reverse (or uphill) diffusion $(-\mathbf{J}_2 \times \partial_x\xi_2 < 0)$ is observed, while at the time $t = t_1$ or t_2, the osmotic diffusion $(\partial_x\xi_2 = 0,\ \mathbf{J}_2 \neq 0)$ can be observed, and at the time $t = t_3$, one can observe the phenomenon of diffusion barrier $(\partial_x\xi_2 \neq 0,\ \mathbf{J}_2 = 0)$. We refer the reader to Ref. [2] for more physical explanations on these curious phenomena.

Finally, we would also like to point out that when the time t is large enough, the problem would reach a steady state, and simultaneously, the diffusion flux and mole fraction gradient would become zero [see Figs. 8(b), 8(c) 9(b), and 9(c)].

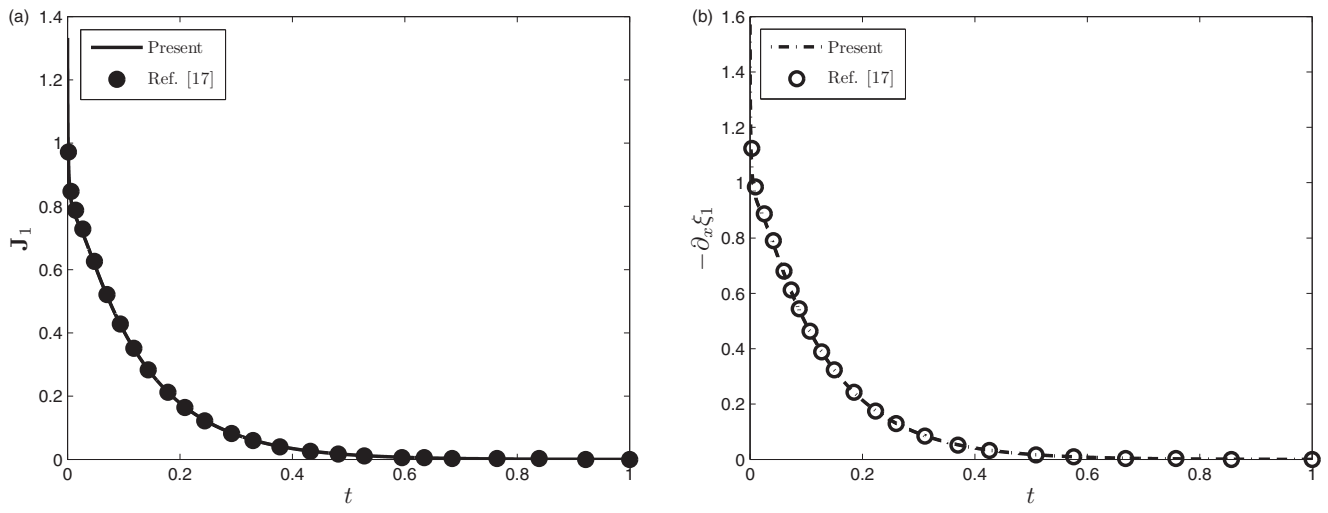

FIG. 6. The diffusion flux $\mathbf{J}_1$ and the negative of mole fraction gradient $(-\partial_x\xi_1)$ at different time $(x = 0.72)$.

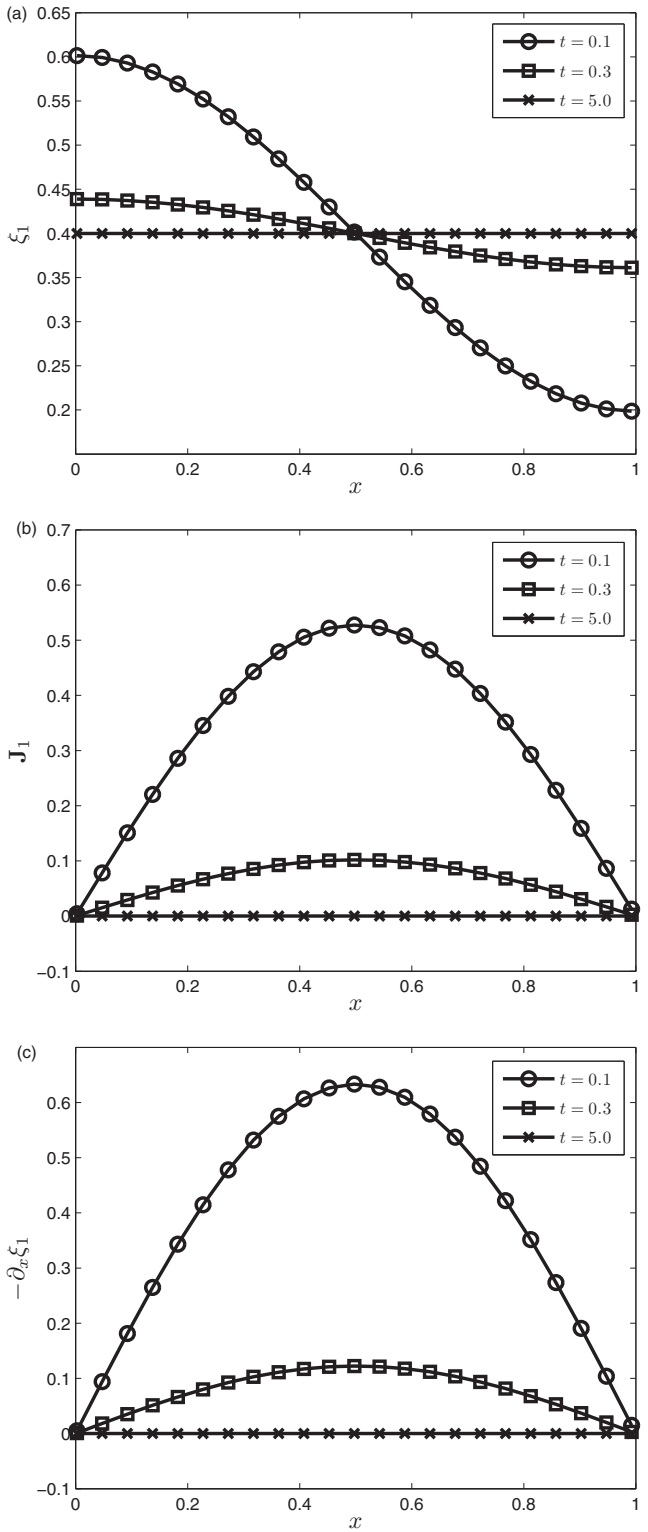

FIG. 8. The distributions of mole fraction ξ_1, diffusion flux $\mathbf{J}_1$ and negative of mole fraction gradient $(-\partial_x \xi_1)$ at different time.

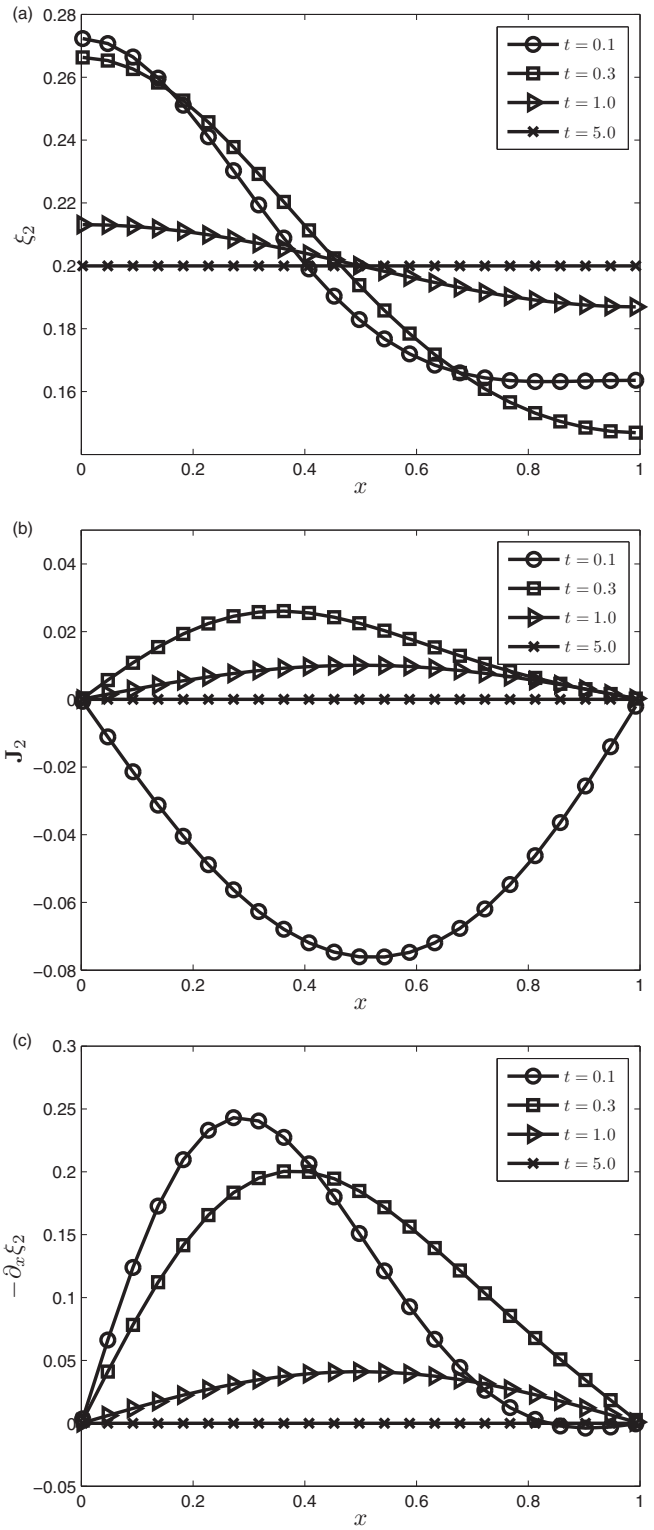

FIG. 9. The distributions of mole fraction ξ_2, diffusion flux $\mathbf{J}_2$ and negative of mole fraction gradient $(-\partial_x \xi_2)$ at different time.

C. Three-component diffusion in the Loschmidt tube

Arnold and Toor [11] investigated the unsteady diffusion of three components in a Loschmidt tube (see Fig. 10 where the schematic of the problem is presented) with the length (L) determined by $(L/\pi)^2 = 1/60$ m^2, and also found some interesting diffusion phenomena. The system they considered is composed of methane (CH_4, species 1), argon (Ar, species 2), and hydrogen (H_2, species 3), and the binary diffusivities among different species are $D_{12} = 21.57\,\text{mm}^2/\text{s}$, $D_{13} =$

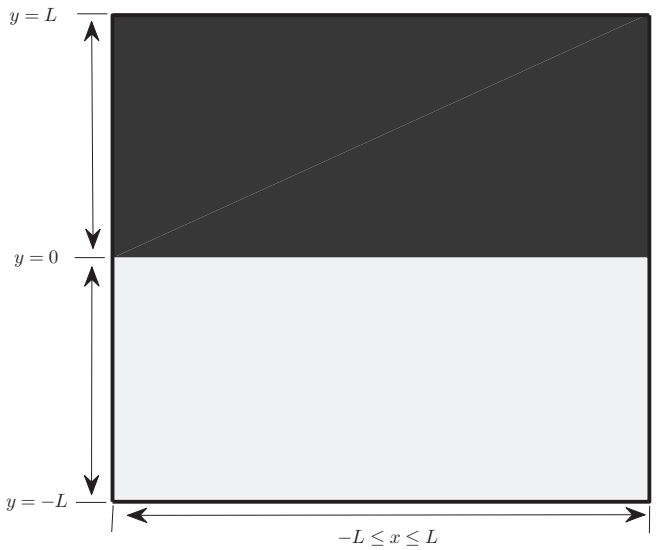

FIG. 10. Schematic of the three-component diffusion in the Loschmidt tube.

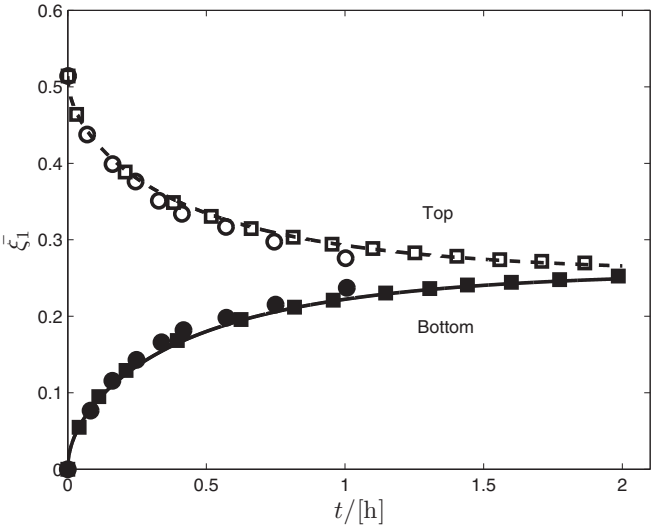

FIG. 11. The average mole fraction $\bar{\xi}_1$ at different time (Solid and dashed lines: Present results; ● and ◯: Experimental data [1]; ■ and □: Linearized theory [1]; h: hour).

$77.16\,\mathrm{mm}^2/\mathrm{s}$, and $D_{23} = 83.35\,\mathrm{mm}^2/\mathrm{s}$ [1,11]. We note that this problem is more complicated than the one above, since the diffusion equations for three species are fully coupled. The initial and boundary conditions of the problem are given by [1,11]

$$0 \leqslant y \leqslant L : \xi_1 = 0.515, \quad \xi_2 = 0.485, \quad \xi_3 = 0.0, \quad (74a)$$

$$-L \leqslant y \leqslant 0 : \xi_1 = 0.0, \quad \xi_2 = 0.509, \quad \xi_3 = 0.491, \quad (74b)$$

$$y = \pm L, \quad \frac{\partial \xi_i}{\partial y} = 0 \ (i = 1,\ 2,\ 3), \quad (75)$$

$$x = \pm L, \quad \xi_i|_{x=-L} = \xi_i|_{x=L} \ (i = 1,\ 2,\ 3). \quad (76)$$

Before performing simulations, we first introduce the following dimensionless parameters:

$$\bar{x} = \frac{x}{L_{\mathrm{ref}}}, \quad \bar{y} = \frac{y}{L_{\mathrm{ref}}}, \quad \bar{t} = \frac{t}{t_{\mathrm{ref}}}, \quad \bar{D}_{ij} = \frac{D_{ij} t_{\mathrm{ref}}}{L_{\mathrm{ref}}^2}, \quad (77)$$

where $L_{\mathrm{ref}} = L = 100\pi \times \sqrt{1/60}$ cm, $t_{\mathrm{ref}} = L_{\mathrm{ref}}^2$ s/cm^2. Based on above dimensionless parameters, the dimensionless length of Loschmidt tube and the dimensionless diffusivities can be determined as

$$\bar{L} = 1.0, \quad \bar{D}_{12} = 0.2157, \quad \bar{D}_{13} = 0.7716, \quad \bar{D}_{23} = 0.8335. \quad (78)$$

Similar to the above problem, the lattice size 200×200 is still applied in our simulations, and to give a comparison between the present results and some available work [1,11], here we also measured the average mole fractions $\bar{\xi}_i$ $(i = 1,\ 2)$ in the bottom and top parts of Loschmidt tube,

$$\text{Bottom: } \bar{\xi}_i = \frac{1}{2L^2} \int_{x=-L}^{L} \int_{y=-L}^{0} \xi_i dx dy,$$

$$\text{Top: } \bar{\xi}_i = \frac{1}{2L^2} \int_{x=-L}^{L} \int_{y=0}^{L} \xi_i dx dy, \quad (79)$$

and presented the results in Figs. 11 and 12. From these two figures, one can observe that our results are in agreement with the available experimental data and linearized theory [1].

In addition, it is also found from Fig. 11 that the average mole fraction $\bar{\xi}_1$ in top part of the Loschmidt tube decreases with the increase of time, while the average mole fraction $\bar{\xi}_1$ in bottom tube shows an opposite trend. Actually, if the time is large enough (e.g., $t = 5.0$ h, h denotes the word "hour"), the average values of mole fraction $\bar{\xi}_1$ in the bottom and top parts of the Loschmidt tube would reach to its equilibrium value $\xi_1^* = 0.2575$, which can be seen clearly from the results in Fig. 13(a). We also noted that although there are cross effects for the mole faction ξ_1, the changes of its average values are similar to theory based on the Fick's law.

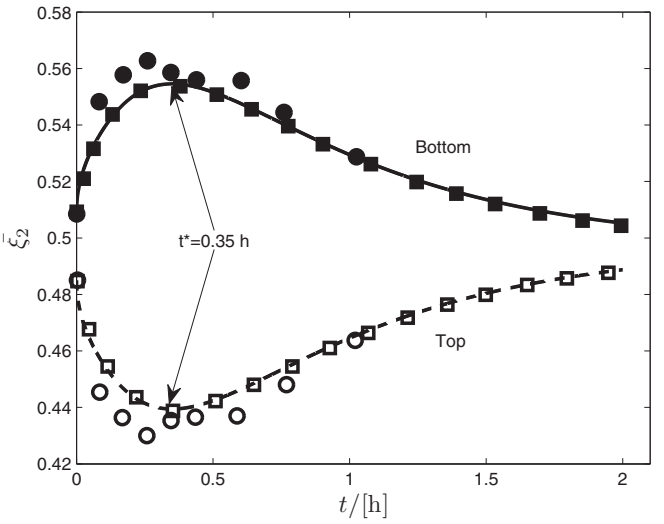

FIG. 12. The average mole fraction $\bar{\xi}_2$ at different time (Solid and dashed lines: Present results; ● and ◯: Experimental data [1]; ■ and □: Linearized theory [1]).

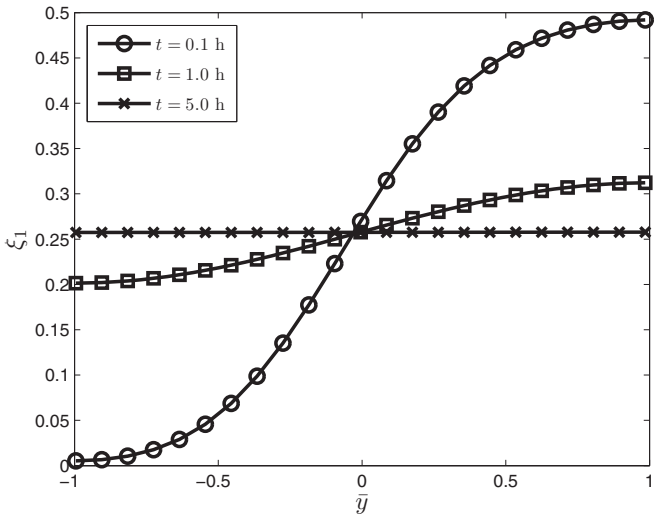

FIG. 13. The profiles of mole fraction $\bar{\xi}_1$ along y direction.

Figure 12 shows the change of the average mole fraction $\bar{\xi}_2$ in time. As seen from this figure, the average mole fraction $\bar{\xi}_2$ in the bottom part of the Loschmidt tube first increases and is up to the maximum value at the time $t* = 0.35$ h, then it begins to decrease, and would reach to its equilibrium value $\xi_2^* = 0.497$ when the time is large enough (see Fig. 14). However, the average mole fraction $\bar{\xi}_2$ in the top part of the Loschmidt tube presents an opposite trend during the time evolution, namely, it first decreases before $t = t*$, then begins to increase when $t > t*$, and approaches to its equilibrium value $\xi_2^* = 0.497$ as time goes on. Compared to the average mole fraction $\bar{\xi}_1$, these curious results of the average mole fraction $\bar{\xi}_2$ are caused by the cross effects among different species, which can be confirmed by Eq. (15).

In addition, we also presented the profiles of mole fractions ξ_1 and ξ_2 along y direction in Figs. 13 and 14. Similar to the results in Figs. 11 and 12, the mole fraction ξ_1 in top part of the Loschmidt tube decreases with the increase of time, while the mole fraction ξ_1 in bottom part of the Loschmidt tube increases in time, and finally both of them reach to the equilibrium value $\xi_1^* = 0.2575$ (see Fig. 13). However, the mole fraction ξ_2 shows some curious results although it approaches to the equilibrium value $\xi_2^* = 0.497$ with the increase of time. At the beginning, the distribution of mole fraction ξ_2 in the Loschmidt tube is not far from its equilibrium state ($\xi_2^* = 0.497$), while under the cross effect caused by other species, the larger mole fraction ξ_2 in the bottom part of the Loschmidt tube further increases, and simultaneously, the smaller mole fraction ξ_2 in top part of the Loschmidt tube oppositely decreases when the time is less than a critical value (see the results at $t = 0.1$ h, 0.3 h in Fig. 14). Then the mole fraction ξ_2 in bottom part of the Loschmidt tube begins to decrease, and the mole fraction ξ_2 in top part of the Loschmidt tube increases, and finally they would reach to the equilibrium value $\xi_2^* = 0.497$ (see the results at $t = 5.0$ h in Fig. 14).

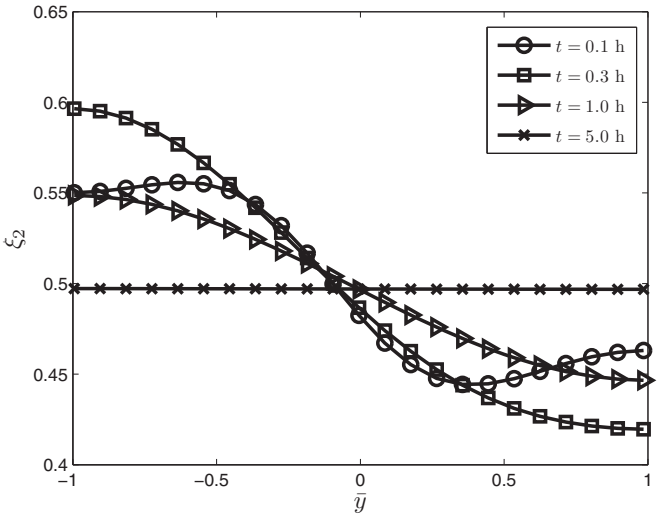

FIG. 14. The profiles of mole fraction $\bar{\xi}_2$ along y direction.

V. CONCLUSIONS

In this work, we first developed a MS-theory-based MRT-LB model for the diffusion in multicomponent mixtures with zero total molar flux and constant total molar concentration, and also performed a Chapman-Enskog analysis to show that the MS-theory-based diffusion equations can be correctly recovered from present MRT-LB model. Compared to the available LB models based on kinetic theory, the present LB model is much simpler, and does not need to apply any interpolations or finite-difference techniques for the multicomponent diffusion problems with different molecular weights. Then we also tested the developed LB model with some benchmark problems, and found the present results agree well with the analytical solutions, available numerical solutions, the experimental data and/or the approximated linear theory. Besides, we would also like to emphasize that the present LB model can also accurately capture the interesting diffusion phenomena (osmotic diffusion, reverse diffusion and diffusion barrier) inherent in the multicomponennt systems.

Finally, it should be noted that in this work, we only consider the diffusion process in the multicomponennt system. In reality, however, the convection (including diffusion and advection) process, as one of the major types of mass transfer, is more prevalent, and would be investigated in a future work.

ACKNOWLEDGMENTS

The authors thank the anonymous referees for their valuable comments and suggestions that improved the quality of this work. This work was financially supported by the National Natural Science Foundation of China (Grants No. 51576079 and No. 51776068) and the National Key Research and Development Program of China (Grant No. 2017YFE0100100).

[1] R. Taylor and R. Krishna, *Multicomponent Mass Transfer* (John Wiley & Sons, New York, 1993).
[2] R. Krishna and J. A. Wesselingh, Chem. Eng. Sci. **52**, 861 (1997).
[3] J. A. Wesselingh and R. Krishna, *Mass Transfer in Multicomponent Mixtures* (Delft University Press, Delft, 2000).
[4] C. Bao, Y. Wang, D. Feng, Z. Jiang, and X. Zhang, Prog. Energy Combust. Sci. **66**, 83 (2018).
[5] R. B. Bird, W. E. Stewart, and E. N. Lightfoot, *Transport Phenomena* (John Wiley & Sons, New York, 2002).
[6] A. Fick, Phil. Mag. **10**, 30 (1855).
[7] J. C. Maxwell, Phil. Trans. R. Soc. Lond. **157**, 49 (1867).
[8] V. J. Stefan, Akad. Wiss. Wien **63**, 63 (1871).
[9] H. L. Toor, A. I. Ch.E. J. **3**, 198 (1957).
[10] J. B. Duncan and H. L. Toor, A. I. Ch.E. J. **8**, 38 (1962).
[11] K. R. Arnold and H. L. Toor, A. I. Ch.E. J. **13**, 909 (1967).
[12] H. L. Toor, A. I. Ch.E. J. **10**, 448 (1964).
[13] W. E. Stewart and R. Prober, Ind. Eng. Chem. Fundam. **3**, 224 (1964).
[14] T. Veltzke, L. Kiewidt, and J. Thöming, A. I. Ch.E. J. **61**, 1404 (2015).
[15] P. S. Weber and D. Bothe, A. I. Ch.E. J. **62**, 2929 (2016).
[16] V. Giovangigli, *Multicomponent Flow Modeling* (Birkhäuser, Boston, 1999).
[17] J. Geiser, Cogent Math. **2**, 1092913 (2015).
[18] W. Wangard, III, D. S. Dandy, and B. J. Miller, J. Comput. Phys. **174**, 460 (2001).
[19] L. Boudin, B. Grec, and F. Salvarani, Discrete Contin. Dyn. Syst.-Ser. B **17**, 1427 (2012).
[20] S. Mazumder, J. Comput. Phys. **212**, 383 (2006).
[21] A. Kumar and S. Mazumder, Int. J. Numer. Meth. Fluids **64**, 409 (2010).
[22] K. S. C. Peerenboom, J. van Dijk, J. H. M. ten Thije Boonkkamp, L. Liu, W. J. Goedheer, and J. J. A. M. van der Mullen, J. Comput. Phys. **230**, 3525 (2011).
[23] K. S. Gandhi, A. I. Ch.E. J. **58**, 3601 (2012).
[24] A. Spille-Kohoff, E. Preuß, and K. Böttcher, Int. J. Heat Mass Transf. **55**, 5373 (2012).
[25] M. Woo, M. Wörner, S. Tischer, and O. Deutschmann, Heat Mass Transf. **54**, 697 (2018).
[26] L. Boudin, D. Götz, and B. Grec, Proc. ESAIM **30**, 90 (2010).
[27] K. Böttcher, Int. J. Heat Mass Transf. **53**, 231 (2010).
[28] M. McLeod and Y. Bourgault, Comput. Methods Appl. Mech. Engrg. **279**, 515 (2014).
[29] A. C. Faliagas, J. Comput. Phys. **308**, 322 (2016).
[30] M. Hirschler, W. Säckel, and U. Nieken, Int. J. Heat Mass Transf. **103**, 548 (2016).
[31] S. Chen and G. Doolen, Annu. Rev. Fluid Mech. **30**, 329 (1998).
[32] S. Succi, *The Lattice Boltzmann Equation for Fluid Dynamics and Beyond* (Oxford University Press, Oxford, 2001).
[33] U. Frisch, B. Hasslacher, and Y. Pomeau, Phys. Rev. Lett. **56**, 1505 (1986).
[34] X. He and L.-S. Luo, Phys. Rev. E **56**, 6811 (1997).
[35] Z. Guo and C. Shu, *Lattice Boltzmann Method and Its Applications in Engineering* (World Scientific, Singapore, 2013).
[36] T. Krüger, H. Kusumaatmaja, A. Kuzmin, O. Shardt, G. Silva, and E. M. Viggen, *The Lattice Boltzmann Method: Principles and Practice* (Springer, Switzerland, 2017).
[37] L.-S. Luo and S. S. Girimaji, Phys. Rev. E **67**, 036302 (2003).
[38] M. E. McCracken and J. Abraham, Phys. Rev. E **71**, 046704 (2005).
[39] A. Xu, Phys. Rev. E **71**, 066706 (2005).
[40] Z. Guo and T. S. Zhao, Phys. Rev. E **71**, 026701 (2005).
[41] P. Asinari, Phys. Rev. E **73**, 056705 (2006).
[42] P. Asinari and L.-S. Luo, J. Comput. Phys. **227**, 3878 (2008).
[43] P. Asinari, Phys. Rev. E **80**, 056701 (2009).
[44] L. Zheng, Z. Guo, B. Shi, and C. Zheng, Phys. Rev. E **81**, 016706 (2010).
[45] S. Arcidiacono, J. Mantzaras, S. Ansumali, I. V. Karlin, C. E. Frouzakis, and K. B. Boulouchos, Phys. Rev. E **74**, 056707 (2006).
[46] S. Arcidiacono, I. V. Karlin, J. Mantzaras, and C. E. Frouzakis, Phys. Rev. E **76**, 046703 (2007).
[47] X. Shan and G. Doolen, J. Stat. Phys. **81**, 379 (1995).
[48] X. Shan and G. Doolen, Phys. Rev. E **54**, 3614 (1996).
[49] Z. Chai and T. S. Zhao, Acta Mech. Sin. **28**, 983 (2012).
[50] M. R. Swift, E. Orlandini, W. R. Osborn, and J. M. Yeomans, Phys. Rev. E **54**, 5041 (1996).
[51] K. S. Ridl and A. J. Wagner, Phys. Rev. E **98**, 043305 (2018).
[52] A. S. Joshi, K. N. Grew, A. A. Peracchio, and W. K. S. Chiu, J. Power Sources **164**, 631 (2007).
[53] P. Asinari, M. C. Quaglia, M. R. von Spakovsky, and B. V. Kasula, J. Power Sources **170**, 359 (2007).
[54] S. H. Kim and H. Pitsch, J. Electro. Soc. **156**, B673 (2009).
[55] P. Rama, Y. Liu, R. Chen, H. Ostadi, K. Jiang, Y. Gao, X. Zhang, R. Fisher, and M. Jeschke, Energy Fuels **24**, 3130 (2010).
[56] Z.-X Tong, Y.-L. He, L. Chen, and T. Xie, Comput. Fluids **105**, 155 (2014).
[57] S. A. Hosseini, N. Darabiha, and D. Thévenin, Physica A **499**, 40 (2018).
[58] X. Meng and Z. Guo, Int. J. Heat Mass Transf. **100**, 767 (2016).
[59] Z. Chai and T. S. Zhao, Phys. Rev. E **87**, 063309 (2013).
[60] Z. Chai and T. S. Zhao, Phys. Rev. E **90**, 013305 (2014).
[61] S. Chapman and T. G. Cowling, *The Mathematical Theory of Non-Uniform Gases* (Cambridge University Press, Cambridge, 1970).
[62] D. Bothe, in *Parabolic Problems*, Progress in Nonlinear Differential Equations and Their Applications, edited by J. Escher, P. Guidotti, M. Hieber, P. Mucha, J. W. Prüss, Y. Shibata, G. Simonett, C. Walker, and W. Zajaczkowski (Springer, Basel, AG, 2011), Vol. 80, pp. 81–93.
[63] L. Chen, Q. Kang, Y. Mu, Y.-L. He, and W.-Q. Tao, Int. J. Heat Mass Transfer **76**, 210 (2014).
[64] H. Huang, M. Sukop, and X.-Y. Lu, *Multiphase Lattice Boltzmann Methods: Theory and Applications* (John Wiley & Sons, Ltd, Chichester, 2015).
[65] Q. Li, K. H. Luo, Q. J. Kang, Y. L. He, Q. Chen, and Q. Liu, Prog. Energy Combust. Sci. **52**, 62 (2016).
[66] H. Liu, Q. Kang, C. R. Leonardi, S. Schmieschek, A. Narváez, B. Jones, J. R. Williams, A. J. Valocchi, and J. Harting, Comput. Geosci. **20**, 777 (2016).
[67] A. Xu, W. Shyy, and T. S. Zhao, Acta Mech. Sin. **33**, 555 (2017).
[68] S. P. Dawson, S. Chen, and G. D. Doolen, J. Chem. Phys. **98**, 1514 (1993).
[69] D. Wolf-Gladrow, J. Stat. Phys. **79**, 1023 (1992).
[70] C. Huber, B. Chopard, and M. Manga, J. Comput. Phys. **229**, 7956 (2010).
[71] I. Ginzburg, Adv. Water Resour. **28**, 1171 (2005).

[72] B. Chopard, J. L. Falcone, and J. Latt, Eur. Phys. J. Special Topics **170**, 245 (2009).
[73] B. Shi and Z. Guo, Phys. Rev. E **79**, 016701 (2009).
[74] H. Yoshida and M. Nagaoka, J. Comput. Phys. **229**, 7774 (2010).
[75] L. Li, R. Mei, and J. F. Klausner, Int. J. Heat Mass Transf. **67**, 338 (2013).
[76] Z. Chai, B. Shi, and Z. Guo, J. Sci. Comput. **69**, 335 (2016).
[77] O. Aursjø, E. Jettestuen, J. L. Vinningland, and A. Hiorth, J. Comput. Phys. **332**, 363 (2017).
[78] Z. Chai, D. Sun, H. Wang, and B. Shi, Int. J. Heat Mass Transf. **122**, 631 (2018).
[79] Y. H. Qian, D. d'Humières, and P. Lallemand, Europhys. Lett. **17**, 479 (1992).
[80] I. Ginzburg, F. Verhaeghe, and D. d'Humières, Commun. Comput. Phys. **3**, 427 (2008).
[81] D. d'Humières, in *Rarefied Gas Dynamics: Theory and Simulations*, Prog. Astronaut. Aeronaut., edited by B. D. Shizgal and D. P. Weave (AIAA, Washington, DC, 1992), Vol. 159, pp. 450–458.
[82] P. Lallemand and L.-S. Luo, Phys. Rev. E **61**, 6546 (2000).
[83] L.-S. Luo, W. Liao, X. Chen, Y. Peng, and W. Zhang, Phys. Rev. E **83**, 056710 (2011).
[84] S. Cui, N. Hong, B. Shi, and Z. Chai, Phys. Rev. E **93**, 043311 (2016).
[85] C. Pan, L.-S. Luo, and C. T. Miller, Comput. Fluids **35**, 898 (2006).
[86] Z. Chai, C. Huang, B. Shi, and Z. Guo, Int. J. Heat Mass Transf. **98**, 687 (2016).
[87] X. Yang, B. Shi, and Z. Chai, Phys. Rev. E **90**, 013309 (2014).
[88] I. Ginzburg, Adv. Water Resour. **28**, 1196 (2005).
[89] T. Zhang, B. Shi, Z. Guo, Z. Chai, and J. Lu, Phys. Rev. E **85**, 016701 (2012).
[90] Q. Chen, X. Zhang, and J. Zhang, Phys. Rev. E **88**, 033304 (2013).
[91] J. Crank, *The Mathematics of Diffusion* (Clarendon Press, Oxford, 1975).